Structure and Reactions of Carbon and Hydrogen on Ru(0001): A Scanning Tunneling Microscopy Study

Tomoko K. Shimizu,[1,2,] Aitor Mugarza,[1,#] Jorge I. Cerdá[3], and Miquel Salmeron[1,2]*

1. Materials Sciences Division, Lawrence Berkeley National Laboratory, Berkeley, CA 94720, USA

2. Materials Science and Engineering Dept., University of California, Berkeley, CA 94720, USA

3. Instituto de Ciencia de Materiales de Madrid, ICMM-CSIC, Cantoblanco, 28049 Madrid, Spain

Corresponding author E-mail: MBSalmeron@lbl.gov

Abstract

The interaction between carbon and hydrogen atoms on a Ru(0001) surface was studied using scanning tunneling microscopy (STM), Density Functional Theory (DFT) and STM image calculations. Formation of CH species by reaction between adsorbed H and C was observed to occur readily at 100 K. When the coverage of H increased new complexes of the form CH+nH (n = 1, 2 and 3) were observed. These complexes, never observed before, might be precursors for further hydrogenation reactions. DFT analysis reveals that a considerable energy barrier exists for the CH+H → CH_2 reaction.

[*] Current address: Surface Chemistry Lab., RIKEN (The institute of physical and chemical research), 2-1 Hirosawa, Wako, Saitama, 351-0198, Japan.

[#] Current address: Centre d'Investigació en Nanociència i Nanotecnologia CIN2 (ICN-CSIC), Campus UAB, 08193 Bellaterra Spain.

1. Introduction

The interaction between carbon and hydrogen to form hydrocarbon species is important in many chemical reactions, including Fischer-Tropsch synthesis, whereby coal or coke is transformed into methane and gasolines [1]. The mechanism of the reaction has been the subject of extensive study [2-10]. Although the overall reaction is simply written as: $nCO+(2n+1)H_2 = nH_2O+C_nH_{2n}+2$, it involves many parallel and intermediate steps, such as CO activation, H_2 dissociation, hydrocarbon coupling, and hydrogenation of unsaturated hydrocarbons. It is believed that a particular form of adsorbed carbon is methanated through a series of hydrogenation reactions of intermediate CH_x fragments [2-4]. These species adsorbed on various metal surfaces have been studied using, for example, high resolution electron energy loss spectroscopy (HREELS) [7-9, 11-15], reflection adsorption infrared spectroscopy (RAIRS) [16] and temperature programmed desorption (TPD) [7-9, 13]. Although CH, CH_2 and/or CH_3 were observed after dissociative adsorption or thermal decomposition of larger hydrocarbons [7-9, 14-16], only CH could be formed by the reaction of atomic carbon and hydrogen [11-13, 16], suggesting the high stability of CH. Because CH was also theoretically found to be most stable among the CH_x species on Ru [5, 6], which exhibits the highest catalytic activity in Fischer-Tropsch synthesis, hydrocarbon chain-growth using CH as a primary monomer unit has been proposed [10].

To learn more about the atomic scale details of the reactions between C and H, we have performed scanning tunneling microscopy (STM) experiments on a Ru(0001) surface in ultra-high vacuum (UHV). Although this environment is far from that used in industry, it allows us to determine the structure, stability and adsorption site of many species that play important roles in the reaction. With the help of DFT-based calculations and STM simulations, we are able to determine the geometrical configurations of C and H atoms and the species they form, as well as to estimate the strength of the interactions involved. We found that CH is the most stable unit, forming readily even at 100 K. We also found that

with additional H on the surface CH forms complexes with up to three H atoms. These previously unknown complexes are possible intermediates in the series of additive reactions leading to methane and higher hydrocarbon formation.

2. Experimental

The experiments were carried out in a home-built liquid helium cooled STM instrument [17, 18]. Data collection was always carried out at 6 K with a base pressure below 2×10^{-11} Torr using electrochemically etched W tips cleaned by field-emission in UHV. A single crystal Ru(0001) sample (5mm×5mm×2mm) was cleaned by several cycles of Ar^+ sputtering at 1 keV and annealing to 1500 K by electron-bombardment. After the sputter-anneal cycles or after each STM experiment, the sample was heated and cooled from 750 K to 1500 K in an O_2 atmosphere of $1\text{-}2 \times 10^{-7}$ Torr and finally annealed to 1650 K to remove excess O. The carbon atoms on the Ru surface were produced by segregation from the bulk during the high temperature annealing. The concentration was always around 3 % of a monolayer (0.03 ML). Atomic H was obtained either by dissociative adsorption of H_2 introduced via a leak valve followed by annealing above 100 K or by thermal dissociation of co-adsorbed H_2O above 140 K.

3. Theoretical

Calculations involving a Ru(0001) slab with H and C species adsorbed in different forms and configurations were performed within the DFT formalism, using the GGA [19] approximation and the SIESTA code [20]. In all cases, the simulation cell was p(4×4) relative to the Ru(0001) lattice and the metal surface was modeled by a 3-layer slab. All other calculation parameters were set to similar values as those employed in Ref. [17]. We constructed the pseudopotentials following the Troullier-Martins[21] scheme, and used a double zeta polarized (DZP) AO basis set for all atoms except for the Ru d states, which were described by a single zeta shell. The radial extension of the orbitals was set according to a confinement energy cost of 100 meV, and the accuracy in the real-space 3-center integrals was set defining a mesh cut-off of 200 Rydbergs [20]. The surface Brillouin Zone integration comprised

4 k-points, corresponding to 64 k-points of the Ru (1×1) lattice. All atoms in the cell were allowed to relax until the forces were smaller than 0.05 eV/Å except for the bottom Ru layer, which was fixed to the bulk geometry. We have checked, for selected structures, that our conclusions are unchanged if better converged parameters are employed (more complete AO basis set, higher resolution in the real space grid, larger k-sampling or an additional Ru layer at the bottom of the slab).

STM simulations were performed for many of the DFT optimized structures, although we will only present some representative cases. The simulations were performed by constructing an infinite surface using the DFT derived coordinates for the surface atoms and a semi-infinite block representing the tip terminated with a sharp apex. The elastic current flowing from tip to sample (or vice versa) was calculated using Green's function techniques [22]. The apex-sample normal distance at each pixel was adjusted until the desired current value was obtained. All simulations were performed assuming 1 nA fixed tunneling current and 100 mV sample bias voltage, which are typical tunneling conditions used in the experiments. Given the complexity of the STM system, the SIESTA *ab initio* Hamiltonian is replaced by the semi-empirical Extended Hückel Theory (EHT), after fitting the EHT parameters in order to reproduce the *ab initio* surface electronic structure [23].

4. Results and discussion

4.1. Formation of CH from C and H

Figure 1 (a) shows a 4 nm ×4 nm STM image of the Ru surface containing approximately 0.03 ML of C atoms prepared as described in the experimental section. The C atoms appear as depressions 30-45 pm deep and approximately 0.5 nm wide. The depth and shape (circular or triangular) depend on the tip conditions. The corrugation of the Ru atoms is low, around 2 to 4 pm under our imaging conditions, and they were not always resolved in the images. As we have shown in a previous paper [17], the C atoms are located on hcp hollow sites of the Ru(0001) surface, where they form strong bonds with the metal atoms. This is consistent with the fact that surface diffusion was never observed during the experiments. After addition of H, either from H_2 dissociative adsorption or from dissociation of co-adsorbed water

after heating above 140 K, many of the C atoms changed their appearance into a depression with a central maximum, as shown in Figure 1 (b). We had previously identified them as CH adsorbed at hcp hollow sites [17]. In addition, small shallow depressions about 30 pm deep are also visible, which correspond to H atoms adsorbed at fcc hollow sites of the Ru(0001) surface [17, 24-30].

Figures 2 and 3 show images from experiments where additional H_2O was adsorbed at 140 K followed by annealing to 180 K. This resulted in a surface covered by various species, including CH (~0.03 ML, from the reaction of C and H), non-reacted C (less than 0.01 ML), O (~0.04 ML, as single atoms or forming small 2×2 clusters), and H atoms (~0.05 ML). The H atoms were sometimes found occupying nearest neighbor sites forming lines. Examples are shown near the center and bottom left of Figure 3. The Ru sites are marked by yellow dots in this figure to aid in the identification of adsorption sites. These positions were established by experiments where atomic resolution of the Ru was obtained, as described in Ref. 17.

In contrast to C, the H atoms are easily perturbed by the electric field of the STM tip, which can cause them to diffuse even when the tip is several nanometers away. For that reason the images need to be acquired by scanning with bias voltages below 70 mV, and gap resistances of 500 MΩ or higher. This type of electric field-induced diffusion has been observed for H on Pd(111) [31]. For example, the area marked in Figure 2 shows a lower concentration of H atoms caused by previous scans in that area at higher electric fields than those used for imaging.

The CH can be dissociated into C and H atoms by tunneling electrons generated from ~ 450 mV voltage pulses, as demonstrated in Figure 4. A voltage ramp from 0 to 500 mV was applied to the tip placed on top of the CH species marked by the arrow in Figure 2 (a). After the ramp, Figure 4 (b) shows that the CH was transformed into atomic C (a roughly triangular depression) while the other CH species remained intact. The high bias voltage necessary for this experiment displaced the H atom away from the image region. By measuring the dependence of the dissociation rate on tunneling current (I_t), one can obtain the number of inelastic electrons (N) involved in the excitation process, which follows the relation $R \sim I_t^N$ [32, 33]. By fitting the data with this expression, we obtain $N = 2.2 \pm 0.4$ for a bias

voltage of 475 mV, as plotted in Figure 5. This indicates that at least two quanta of the C-H stretch oscillation (hν = 372 meV) are needed for the dissociation of CH [8]. The energy barrier for CH dissociation istherefore is between 372 meV and 744 meV. Due to the low dissociation yield, 5×10^{-11} events/electron at I_t =1 nA, the voltage threshold could not be precisely determined and all dissociation events were obtained with voltages above 450 mV.

4.2 Formation of (CH+nH) complexes

In addition to the species described above (CH, C, H, and O), we also found complexes of CH and H. They appear in the images as a bright spot (~10 pm maximum), located at hcp hollow sites surrounded by 1, 2 or 3 dark spots (~30 pm depressions) at nearby fcc hollow sites. Two such complexes are marked with circles in Figure 3. The left column in Figure 6 shows examples of enlarged images of (CH+nH) complexes with n=3 (a), n=2 (b), n=1 (c) and n=0 (d). The distance between the center of the bright spot and each of the 3 dark spots in (a), (b) and (c) is 0.30 ± 0.04 nm, which is close to 0.313 nm, the distance between an hcp hollow site and the second nearest fcc hollow sites. Models of these complexes are shown in the central column of Figure 6. Evidence for the nature of the (CH+nH) complex was obtained by tip manipulation experiments, where voltage pulses as low as 70 mV applied with the tip over the complex could partially or completely remove the surrounding H atoms, leaving behind an isolated CH.

STM simulated images of the (CH+nH) complexes, using the DFT optimized geometries of the models in the central column of Figure 6, are displayed on the right hand side column. As can be seen, the prominent features of the experimental images are reproduced quite well. The calculated topographic corrugations: 10 pm height and 20 pm depth compare reasonably well also with the experimental values, which vary from 0 to 10 pm high at the center and from 15 to 30 pm deep at the perimeter, depending on the tip condition and tunneling parameters.

We have also analyzed other geometrical arrangements of H and CH that can represent some of the observed structures: for example, the linear arrangements of H in Figure 3. A calculated image for this

particular geometry is shown in Figure 7 (b), together with a schematic diagram (c) and an expanded view (a) of the image of Figure 3. Here again the agreement is remarkably good. The tendency of H to align to form one-dimensional chains agrees with IV-LEED experiments of H on Ru(0001) [34], and will be addressed in the next section.

It is possible that the (CH+nH) complexes are precursors for further reaction (CH+nH)→CH_{n+1}, leading to methane formation. Under our H coverage and sample temperature conditions, however, we did not succeed in producing any new species, even by injecting tunneling electrons from the STM tip, which always resulted in diffusion of the surrounding H atoms away from the CH species at voltages above 70 mV, or in CH dissociation for voltages above 450 mV, as stated in the previous section. Annealing the surface to 100-300 K did not produce any further hydrogenation reaction either. During annealing experiments the total coverage of C and CH remained constant at 0.03 ML, a result independent of whether the H was produced by water dissociation or by H_2 dissociation.

5. Energy calculations

The finding that CH is a very stable species is in line with the result obtained by Barteau et al. using HREELS [11, 12] The authors observed CH formation after exposing the surface to H and heating to 370 K. CH_2, CH_3 or CH_4 were not observed under UHV conditions. Using theoretical calculations Ciobica et al. [5, 6] found that CH is the most stable species among all CH_x (x=0-4). When the interaction between CH and H atoms was considered, CH+3H was found to be the most stable among CH_4, CH_3+H, CH_2+2H, CH +3H and C+4H. Their calculated structure for CH+3H is indeed the same as the one we calculated, although a somewhat smaller unit cell was employed in their simulations. The authors also found a relatively high activation barrier from C+4H to CH+3H, around 70 kJ/mol or 725 meV [6]. This does not agree with our findings where CH was formed after annealing a H-covered surface to 100 and up to 260 K. Assuming a pre-exponential value of 10^{13} Hz and a probability of CH formation at 100 K of 1/second (our experimental time scale), the activation energy is estimated to be approximately 260 meV. An activation energy of 725 meV would result in an immeasurably low

probability of reaction in our conditions. However, Ciobica et al. conclusion that CH is more stable than atomic C and H is consistent with our estimate of energy barriers of CH formation (260 meV) and dissociation (higher than 372 meV).

5.1 The CH-H interaction

To gain an understanding of the CH and H interactions leading to the CH+H→CH_2 reaction on the Ru(0001) surface, we performed total energy DFT based calculations as a function of the CH-H distance along the [1100] direction, d_{CH-H}. The CH species was placed on an hcp site in a (4×4) cell, and the H atom on the fcc site 7.91 Å away from it. The H atom was then displaced towards the CH along a straight line in 0.1 Å steps until the separation between the two species was d_{CH-H}=1.5 Å, as indicated by the arrow from the right in Figure 8 (b). For each d_{CH-H} distance, we relaxed all atomic coordinates, except the in-plane H coordinates, and those of the Ru bottom layer (fixed to the Ru bulk positions) [35]. Figure 8 (a) shows the evolution of the total energy E^{Ru}(CH+H) along this trajectory. As expected, we find a minimum at each hollow site, the far fcc site being the most stable, followed by the second nearest neighbor (nn) fcc site, fcc2, and finally the third nn hcp site, hcp3. Diffusion from the fcc2 to the nearby hcp3 position across the bridge site yields a small energy barrier of around 0.13 eV. Diffusion over the top site shown in the graph involved a much larger barrier (around 0.5 eV). When d_{CH-H} becomes less than 3.0 Å, the total energy increases rapidly as the H shifts from the fcc2 site towards the CH over the top site and CH_2 starts to form (at d_{CH-H} ~1.5 Å) (Figure 8 (a)). In principle, one may think that this repulsive interaction is due to the fact that the H needs to cross over a top site, i.e. overcome a large energy barrier of around 0.6 eV, when approaching the CH. When H approaches the CH from the left side in Figure 8, starting at the hcp2 site and over the top site near 3 Å, a shallow minimum is found at the first nn fcc site, fcc1. Although unstable relative to the other fcc sites located farther away, this minimum could possibly be filled at high H coverage, when all other sites are full. It could thus be an intermediate state in the formation of CH_2. We have not found any experimental evidence for this at the

H coverage of this study (<0.25 ML). Experiments to explore the possibility of CH_2 formation at high H coverage are being planned.

We have also calculated the CH-H bond energy in the gas phase (solid line) and that when adsorbed on Ru (dashed line) as a function of the distance as shown in Figure 8 (c). We obtain an almost zero interaction for all d_{CH-H} values in the adsorbed case, meaning that the CH-H bonding interaction on the surface is very small, even attaining negative values (slightly repulsive) for a certain range of distances. In other words, *the Ru surface screens almost completely the CH-H attraction*.

5.2 Effects of H-coverage

The energetic hierarchy among hollow adsorption sites deduced in the previous subsection seems to be in contradiction to the experimental evidence showing that (CH+nH) complexes form quite often. A possible explanation can be sought in the fact that experimentally there is always additional H on the surface around the (CH+nH) complexes. We thus performed total energy calculations for (CH+nH) complexes under various H coverage values, compatible with the (4×4) simulation cell. Assuming that H adsorbs always at fcc sites, and excluding the 3 fcc1 sites surrounding the CH at the hcp position, there are up to 13 fcc sites available in the (4×4) cell. Therefore, for each (CH+nH) complex, the number of additional H atoms in the cell, mH, can be varied from m=0 to 13–n. For each (CH+nH)+mH case, we have performed at least one total energy minimization for a given H arrangement [36].

We define the average H adsorption energy, EH_{ads}^{Ru}, per (CH+nH)+mH configuration as: $EH_{ads}^{Ru}((CH+nH)+mH) = \{ -E^{Ru}((CH+nH)+mH) + E^{Ru}(CH) + (n+m)E^{g}(H)\} / (n+m)$. A summary of these averaged adsorption energies for all the models studied is presented in Figure 9 as a function of (n+m), the total number of H atoms in the cell. Gray, solid, dashed and dotted lines correspond to the most stable configurations found containing a (CH+nH) complex with n=0, 1, 2 and 3, respectively. The additional data points in the graph correspond to alternative, less stable H arrangements. It is immediately apparent that the adsorption energy EH_{ads}^{Ru} decreases by nearly 100 meV from the lowest to the highest coverage. Secondly, at low and medium H coverage, the smaller the n, the more stable is

the system. As can be seen, at high coverage all curves converge to similar values, and the difference between adsorbing H at an fcc2 site or at another fcc position is only a few meV, in the range of the numerical accuracy of the calculations. Such small differences offer a simple explanation to the frequent presence of (CH+nH) complexes on our surface when the concentration of H increases.

The insets in Figure 9 illustrate the H arrangements for three representative cases having n+m=3. Interestingly we find that the most stable configuration involves adjacent H atoms aligned in straight lines linking the CHs. The one dimensional arrangements are slightly more favorable than two dimensional ordered phases (e.g. (2×2) or ($\sqrt{3}\times\sqrt{3}$) H networks). This result is fully consistent with the presence of dark lines in the experimental observation (Figure 3 and 7) as well as an early IV-LEED experiment [34].

6. Conclusions

We have studied the structure and interaction between C and H atoms on Ru(0001) at the single atom level using low temperature STM. The results obtained provide a detailed picture of the species that form, which, in addition to C and H include CH, confirm earlier findings that the most stable species is CH and that it is adsorbed on the hcp hollow site. The easy formation of CH, at temperatures of 100 K indicates that the activation barrier for this reaction is of the order of 260 meV. On the other hand, tunneling electron-induced CH dissociation experiments indicate a higher dissociation energy barrier, between 372 and 744 meV, confirming the higher stability of CH than its reactants C and H.

One of the most interesting findings is the identification of complexes of the form of CH surrounded by 1, 2 and 3 H atoms in the second nearest neighbor fcc positions. These previously unknown complexes are stable and form abundantly when the surface is crowded with H atoms. They are possible intermediate species in the reaction pathway leading to methanation. Under the low temperature (up to 300 K) and low H coverage of the present experiments, however, further reaction to form CH_2, CH_3 and CH_4 was not observed.

The theoretical calculations of total energies for a variety of H and CH geometries, along with the calculated STM images allowed us to draw a detailed picture and to gain a deeper understanding of some of the surface reactions involved in the initial steps of methane and larger hydrocarbon formation.

Acknowledgements

This work was supported by the Director, Office of Science, Office of Basic Energy Sciences, Materials Sciences and Engineering Division, of the U.S. Department of Energy under Contract No. DE-AC02-05CH11231, and by the Spanish Ministry of Science and Technology under Projects No. MAT2007-66719-C03-02 and NAN2004-09125-C07-06. The work of A.M. was financed by the Marie Curie Outgoing International Fellowship, Project No. 514412.

Figures

Figure 1

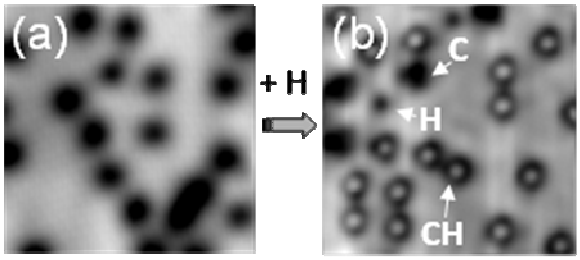

STM images (4 nm × 4 nm) of Ru(0001) acquired at T = 6 K. (a) Surface containing approximately 0.03 ML of C prepared by segregation from the bulk. The C atoms appear as depressions (black spots). (b) After introducing H atoms (from water dissociation in this experiment), C is converted to CH (bright protrusion surrounded by a dark ring). A similar transformation occurs with H obtained from H_2 dissociation. Individual non-reacted H atoms appear as smaller dark spots. Tunneling condition in (a) is V_{sample}=50 mV and I_t=295 pA, and (b) V_{sample}=9 mV and I_t=495 pA. The total z scale is adjusted to be 50 pm in both images.

Figure 2

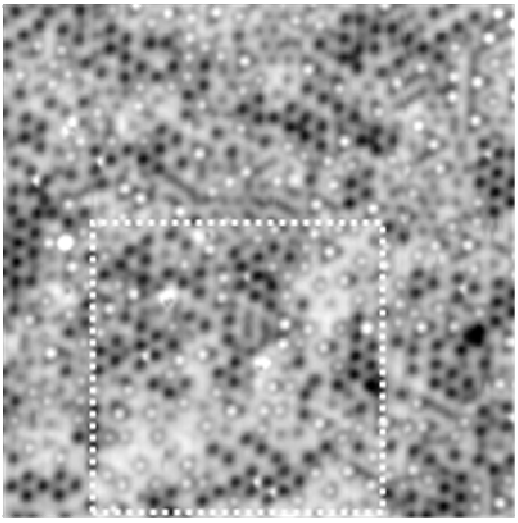

STM image acquired at 6 K (15 nm × 15 nm, V_{sample}=25 mV and I_t=195 pm) after introducing H atoms from water dissociation after heating to 180 K. Oxygen atoms (dark circular depressions forming small 2×2 aggregates), CH, H and (CH+nH) complexes can be observed. The area enclosed within the broken line had been previously scanned at higher bias voltages that caused the displacement of most of the H atoms away from the region.

Figure 3

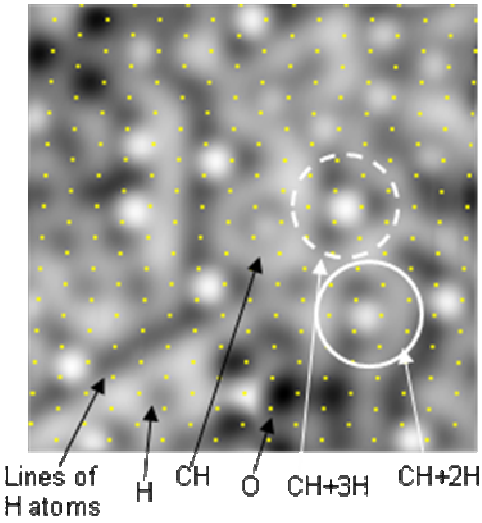

STM image at 6 K (4 nm × 4 nm, V_{sample}=24 mV and I_t=52 pA) showing C, H, CH and (CH+nH) complexes on Ru(0001). The surface was prepared by dosing H_2O at 150 K on the Ru(0001) surface containing 0.03 ML of C, followed by annealing to 200 K. Small dots indicate the position of the Ru atoms. Two circles mark the position of (CH+3H) (top) and (CH+2H) (bottom) complexes. The few O atoms visible at the bottom and top left of the image originated from water dissociation. All species reside on hcp hollow sites, except H which occupies fcc sites. Notice also the dark lines due to H atoms aligned in the compact crystallographic directions near the bottom left and center of the image, connecting (CH+3H) complexes.

Figure 4

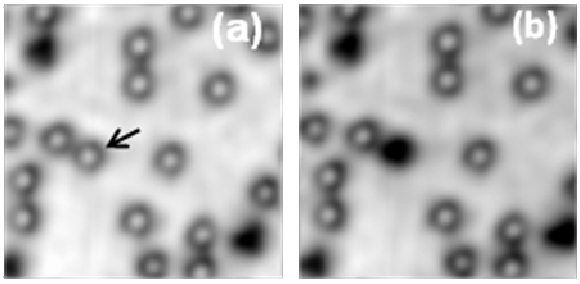

STM images at 6 K (4 nm × 4 nm; V_{sample}=10 mV and I_t=500 pA) acquired before (a) and after (b) CH dissociation induced by applying a voltage ramp from 0 to 0.5 V with an initial set point of 10 mV and 50 pA with the tip stationed over the CH species marked by the arrow in (a). The CH species is transformed to C and the dissociated H has been displaced away from the image by the high electric field from the tip during the voltage ramp.

Figure 5

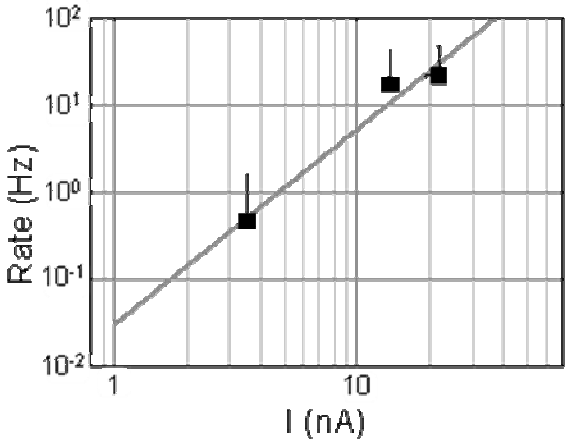

Log-log plot of the CH dissociation rate vs. tunneling current at the time of event (during the pulse). The bias voltage was kept at 475 mV. From the slope of the plot, the rate was found to be proportional to $I^{2.2\pm0.4}$. This indicates that two electrons are necessary to excite two quanta of C-H stretch oscillation, which result in the rupture of the bond.

Figure 6

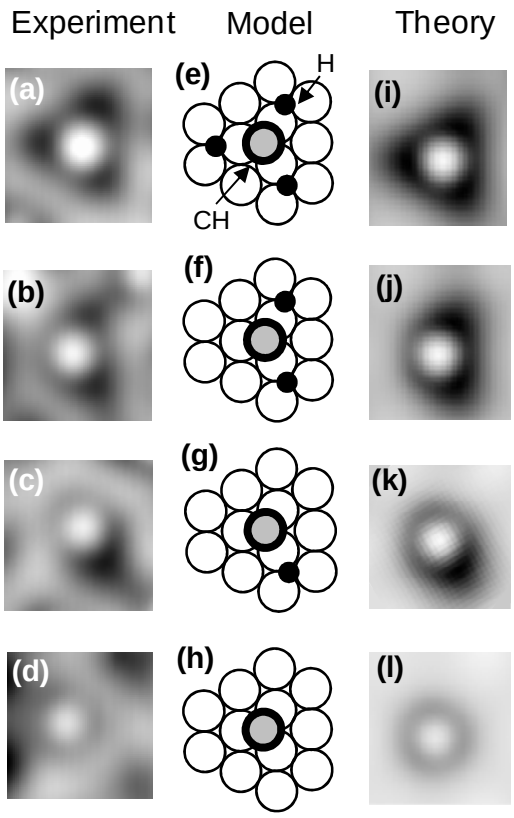

(a)-(c) enlarged STM images (1 nm × 1 nm, V_{sample}=19 mV and I_t=200 pA) showing three (CH+nH) (n=1-3) complexes and CH (d). The gray scale of all four images is adjusted to be 90 pm for easier comparison of contrast. (e)-(h) Schematic models of the geometrical configuration employed to simulate the experimental images. All geometries were optimized by energy minimization in DFT calculations, as explained in the text. (i)-(l) Simulated STM images for each optimized model employing a W tip (tunneling conditions set to V_{sample}=100 mV and I_t=1 nA).

Figure 7

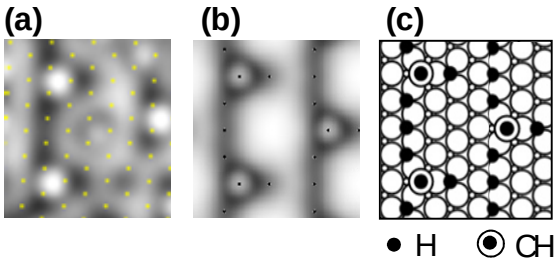

(a) STM image (2 nm × 2 nm, V_{sample}=24 mV and I_t=52 pA) extracted from Figure 3 containing a linear structure of H atoms (vertical dark band connecting 2 CH+3H complexes). The feature in the center is due to a CH species, not H. The location of the H atoms is indicated by the small superimposed yellow dots. (b) Simulated STM image corresponding to the schematic geometrical configuration in (c). Black dots in (b) indicate the site of H and CH.

Figure 8

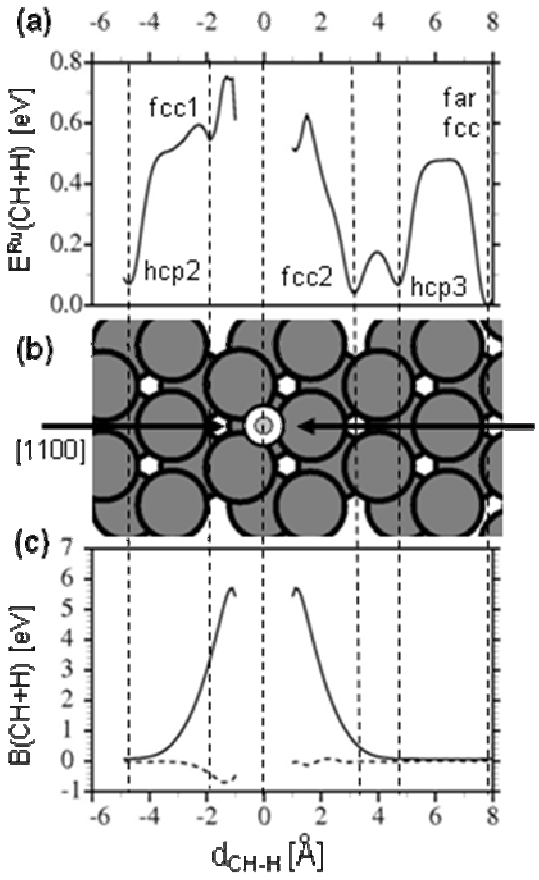

(a) Graph of total energy of the system, $E^{Ru}(CH+H)$, calculated by DFT, as a function of the CH-H distance, d_{CH-H}. The origin of energy has been set at the configuration of the most stable structure, with H at an fcc site far (~8 Å) from the CH. The plotted energy values give the energy difference with respect to this site, with positive values corresponding to less stable arrangements. (b) Sketch of the Ru(0001) surface with the CH adsorbed at the hcp site, corresponding to d_{CH-H}=0. The arrows indicate two H trajectories used in the calculations as it approaches the CH from the right and left directions. (c) Solid line: CH-H bond energy in the gas phase, $B^g(CH+H) = -E^g(CH+H) + E^g(CH) + E^g(H)$, where $E^g(X)$ gives the total energy of species X and the superscript g stands for the gas phase, as a function of the CH-H distance; dashed line: CH-H bond energy with both species adsorbed on the Ru surface, $B^{Ru}(CH+H) = -E^{Ru}(CH+H) + E^{Ru}(H) + E^{Ru}(CH) - E^{Ru}$, where $E^{Ru}(X)$ refers to the total energy of the Ru slab with species X adsorbed on it and E^{Ru} gives the total energy of the bare Ru slab. The formation of a CH-H bond, favorable in the gas phase is suppressed by the presence of Ru.

Figure 9

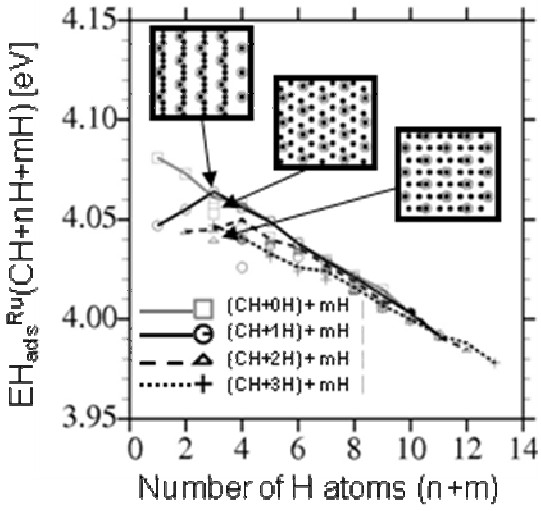

Average adsorption energy per H atom for the Ru(0001)-(4×4)+((CH+nH))+mH systems as a function of the total number of H atoms (n+m) in the cell. Gray, solid, dashed and dotted lines correspond to the most stable configurations found containing a ((CH+nH)) complex with n=0, 1, 2 and 3, respectively. Additional data points are for different, less stable configurations. The insets sketch the H arrangement for three different cases satisfying n+m=3. The linear arrangement of H atoms (top inset) is the most stable of the three.

References

1. V. Ponec, in *Handbook of Heterogeneous Catalysis. Volume 4*, edited by G. Ertl, H. Knozinger and J. Weitkamp (VCH-Wiley, Weinheim, 1997), p. 1876.

2. M. Araki, V. Ponec, J. Catal. **44**, 439 (1976).

3. P. Biloen, W. H. M. Sachtler, Adv. Catal. **30**, 165 (1981).

4. R. A. van Santen, A. de Koster, T. Koerts, Catal. Lett. **7**, 1 (1990).

5. I. M. Ciobîcă, F. Frechard, R. A. van Santen, W. Kleyn, J. Hafner, Chem. Phys. Lett. **331**, 185 (1999).

6. I. M. Ciobîcă, F. Frechard, R. A. van Santen, W. Kleyn, J. Hafner, J. Phys. Chem. B **104**, 3364 (2000).

7. P. M. George, A. R. Averey, W. H. Weinberg, F. N. Tebbe, J. Am. Chem. Soc. **105**, 1393 (1983).

8. M.-C. Wu, D. W. Goodman, J. Am. Chem. Soc. **116**, 1364 (1994).

9. Y. Zhou, M. A. Henderson, W. Feng, J. White, Surf. Sci. **224**, 386 (1989).

10. I. M. Ciobîcă, G. J. Kramer, Q. Ge, M. Neurock, R. A. van Santen, J. Catal. **212**, 136 (2002).

11. M.A. Barteau, J.Q. Broughton, D. Menzel, Appl. Surf. Sci. **19**, 92 (1984).

12. M. A. Barteau, P. Feulner, R. Stencgl, J. Q.Broughton, D. Menzel, J. Catal. **94**, 51 (1985).

13. M. Yu. Smirnov, V. V. Gorodetskii, A. R. Cholach, D. Yu. Zemlyanov, Surf. Sci. **311**, 308 (1994).

14. J. E. Demuth, H. Ibach, Surf. Sci. Lett. **78**, L238 (1978).

15. Q. Y. Yang, K. J. Maynard, A. D. Johnson, S. T. Ceyer, J. Phys. Chem. **102**, 15 (1995).

16. R. Deng, E. Herceg, M. Trenary, Surf. Sci. **573**, 310 (2004).

17. T. K. Shimizu, A. Mugarza, J. I. Cerdá, M. Heyde, Y. Qi,; U. D. Schwarz, D. F. Ogletree, M. Salmeron, J. Phys. Chem. C **112**, 7445 (2008).

18. B. H. Albers, M. Liebmann, T. C. Schwendemann, M. Z. Baykara, M. Heyde, M. Salmeron, E. I. Altman, U. D. Schwarz, Rev. Sci. Instrum. **79**, 033704 (2008).

19. J. P. Perdew, K. Burke, M. Ernzerhof, Phys. Rev. Lett. **77**, 3865 (1996).

20. J. M. Soler, E. Artacho, J. Gale, A. García, J. Junquera, P. Ordejón, D. Sánchez-Portal, J. Phys. Condens. Matter. **14**, 2745 (2002).

21. N. Troullier J. L. Martins, Phys. Rev. B **43**, 1993 (1991).

22. J. I. Cerdá, M. A. Van Hove, P. Sautet, M. Salmeron, Phys. Rev. B **56**, 15885 (1997); see also www.icmm.csic.es/jcerda.

23. J. I. Cerdá, F. Soria, Phys. Rev. B **61**, 7965 (2000).

24. M. Tatarkhanov, F. Rose, E. Fomin, D. F. Ogletree, M. Salmeron, Surf. Sci. **602**, 487 (2008).

25. F. Rose, M. Tatarkhanov, E. Fomin, M. Salmeron, J. Phys. Chem. C **111**, 19052 (2007).

26. M. Lindroos, H. Pfnür, P. Feulner, D. Menzel, Surf. Sci. **180**, 237 (1987).

27. M. Lindroos, H. Pfnür, D. Menzel, Surf. Sci. **192**, 421 (1987).

28. K. L. Kostov, W. Widdra, D. Menzel, Surf. Sci. **560**, 130 (2004).

29. M. Y. Chou, J. R. Chelikowsky, Phys. Rev. Lett. **59**, 1737 (1987).

30. L. Xu, H.Y. Xiao, X. T. Zu, Chem. Phys. **315**, 155 (2005).

31. T. Mitsui, E. Fomin, D.F. Ogletree, M. Salmeron, A.U. Nilekar, M. Mavrikakis, Angew. Chem. Int. Ed. **46**, 5757 (2007).

32. B. Stipe, M. Rezaei, W. Ho, Science **279**, 1907 (1998).

33. H. Ueba, Surf. Rev. Lett. **10**, 771 (2003).

34. G. Held, H. Pfnür, D. Menzel, Surf. Sci. **271**, 21 (1992).

35. Strictly speaking, d_{CH-H} corresponds to the in plane distance from the H to the hcp site. However, for the range of distances considered the C atom never shifted by more than 0.15 Å from the ideal hcp site. Therefore, we may identify d_{CH-H} with the in plane distance between the H and CH.

36. The arrangements of the H atoms inside the cell have been chosen arbitrarily, comprising high and low densely packed configurations or a mixture of both. In some cases we have considered two or three different H configurations with the same n and m values.